PERFORMANCE OF THE TRISTAN-AR MAGNET

K. Egawa, H. Fukuma, Ta. Kubo, N. Kumagai, Y. Takeuchi, K. Endo

JOURNAL DE PHYSIQUE
Colloque C1, supplément au n° 1, Tome 45, janvier 1984

PERFORMANCE OF THE TRISTAN-AR MAGNET

K. Egawa, H. Fukuma, Ta. Kubo, N. Kumagai, Y. Takeuchi and K. Endo

National Laboratory for High Energy Physics, Oho-machi, Tsukuba-gun, Ibaraki-ken, 305, Japan

Résumé - Un système d'aimants pour l'accélérateur accumulateur, TRISTAN-AR, est décrit du point de vue de la fabrication des performances et des propriétés optiques déduites des données de champs magnétiques.

Abstract - A magnet system of the storage accelerator, TRISTAN-AR, is described with respect to the fabrication, performances and beam properties expected from the field data.

The TRISTAN-AR (Accumulation Ring) magnet system /1/ consists of 56 dipoles, 86 quadrupoles, 40 sextupoles and 54 steering dipoles in addition to 56 backleg windings. All magnets allow the pulsatory excitation to afford the electron-positron colliding experiments at the accelerated energy. Both beams are injected at 2.5 GeV and accelerated up to 6.5 GeV. In the case when the AR ring serves as an injector to the TRISTAN main ring, it accelerates up to 8 GeV. Parameters of magnets are given in Table 1.

I - MAGNET SYSTEM

Table 1 Parameters of magnets

	Dipole	Quadrupole		Sextupole		Steering dipole			
		MQ	IQ	SXF	SXD	STV 1	STV 2	STH 1	STH 2
number of magnets	56	78	8	20	20	36	8	2	8
(1) mechanical									
gap height (mm)	60	—	—	—	—	130	154	70	154
bore dia. (mm)	—	80	120	92	92	—	—	—	—
core length (mm)	2 x 1290	500	1100	170	270	250	175	200	75
core crosssection(mm²)	560 x 560	506 x 506	800 x 800	390 x 390		160 x 220	340 x 330	275 x 150	330 x 330
core weight (kg)	6700	1100	5600	130	200	22	66	30	28
coil weight (kg)	600	120	480	12	16	16	66	20	16
turn number of coil (turns/pole)	16	10	17	32	32	2 x 364	2 x 1042	2 x 520	2 x 897
(2) electric and magnetic									
max. current (A)	1805	1340	1340	100	100	± 10	± 10	± 10	± 10
max. field strength	1.15 T	20 T/m	15 T/m	250T/m²	250T/m²	0.035 T	0.09 T	0.09 T	0.07 T
resistance (Ω)	0.014	0.006	0.019	0.1	0.13	2 x 0.86	2 x 1.31	2 x 0.9	2 x 0.9
inductance (H)	0.019	0.006	0.013	0.012	0.018	2 x 0.03	2 x 0.2	2 x 0.1	2 x 0.07

NQ : normal quad, IQ : insertion quad, SXF : hor. sextupole, SXD : ver. sextupole,
STV : ver. steering dipole, STH : hor. steering dipole

Dipole and quadrupole Each dipole has two C-shaped 1.29 m iron cores placed on a common girder at an angle of 3.214 degrees and has a set of common coils. The vertical and horizontal apertures are 60 and 90 mm, respectively. The vertical aperture allows the full coupling ± 10 σ beam size and the horizontal one the zero coupling ± 10 σ beam size at 6.5 GeV including the 9 mm sagitta.
78 normal quadrupoles having 80 mm bore diameter are placed in the regular cells, RF and dispersion suppressor cells. 8 insertion quadrupoles with 120 mm bore diameter are placed in the low ß sections near the interaction points. Both quadrupoles have the symmetric pole profiles because of their good field symmetry. The horizontal and vertical apertures are 69 and 41 mm respectively for the normal quadrupole, while for the insertion quadrupole 104 and 81 mm respectively. The magnets of the storage accelerator are excited with the dc current for a long time. The coil dimensions are so large that the iron core had to be made separable into 4 blocks to accommodate the coils. Both upper two blocks and lower two blocks were bolted and also welded after inserting the coils. However, the upper and lower cores were left separable for the convenience of the vacuum chamber installation.
The cores of both dipole and quadrupole were made of the 0.5 mm thick silicon steel laminations, S23 (grade of the Japanese Industrial Standards). The laminations having the inorganic insulation layers were stacked between the SUS304 end plates and welded to the iron bars on the sides in the stacking fixture. As the magnetic properties of the silicon steel had a directional dependence (magnetic anisotropy), two types of sheets punched parallel (L) and transverse (C) to the rolling direction

with two stamping dies were mixed sheet by sheet automatically before stacking. While for the dipole, the steel sheet was punched so that the flux in the pole ran parallel to the rolling direction which had the largest permeability.
The coils were made of the oxygen free copper hollow conductor and insulated with the semi-cure fiberglass tape pre-pregnated with the radiation resistant epoxy resin. For the ground wrapping, the same tape lined with mica was used. The insulation system will bear the radiation absorption more than 5 x 10^8 rad.

Sextupoles In the AR, the momentum spread of the electron beam is 0.115 % at 6.5 GeV. The chromatic aberration arising from the momentum dependence on the focusing strength of the quadrupole is compensated with the sextupoles. The sextupoles were made of the 0.5 mm thick S30 (JIS) silicon steel. The iron core was composed of six laminated blocks with the lengths of 170 and 270 mm for the sextupole placed near the horizontally and vertically focusing quadrupoles respectively. The coil was made of the 0.65 mm thick anodized Al ribbon with 60 mm width. The Normex 410 sheets were enfolded between the layers to ensure the insulation. The outermost surface of the coil was covered with the Cu strip with the cooling channel.

Steering dipole and backleg winding 44 vertical steering dipoles are used for the vertical orbit control and 10 horizontal steering dipoles and 56 backleg windings wound around the yokes of the main dipoles for the horizontal orbit control. Each steering dipole or backleg winding is energized individually.

II - PERFORMANCES OF MAGNETS

The field properties of all magnets were measured. The field measuring systems were designed to allow the fast and accurate measurements with few persons. The main dipoles were measured statically with the 3 m long flip coil driven with the pulse motors at both ends. The induced voltage was integrated during the rotation of the coil with the accurate integrator and then measured with a digital voltmeter, FLUKE 8502 A. The digital data were stored in the minicomputer, PDP11/34, via GPIB interface in the CAMAC crate /2/. The effect of the inclined two cores was corrected with the data of the point measurements.
The different measurements were made to the quadrupoles, because the rotation of the long twin coils was difficult in the small gap. Placing the long twin coils parallel to the core axis, the field gradients were measured at 10 field levels during a pulsatory excitation. At each predetermined field level the trigger pulse was generated by comparing it with the field gradient of the reference quadrupole which was connected serially to the concerned quadrupole. The trigger pulse was used to measure the instantaneous output of the integrator which integrated the induced voltage of the long twin coils. The remanent field gradient was measured by rotating the same twin coils around the core axis and added to the dynamically measured data. The sextupoles and the steering dipoles were measured with the commercially available rotating coil. The sextupole component was obtained by differentiating twice the raw data.
The field measuring coils were moved automatically providing the accurate number of the driving pulses to the pulse motors through the stepping motor controllers from the computers. A series of measurements was done online for the dipole and the quadrupole. Table 2 gives the summary of the field measurements.

Table 2 Summary of the field measurements

Magnet	Dipole	Quadrupole	Sextupole and steering dipole
Probe	long flip coil	long twin coils	rotating coil
Magnet excitation	static	dynamic	static
Raw data	integrated field strength	integrated field gradient	field strength at each point
Remanent field	included	measured with the supplemental measurement	included
Accuracy	10^{-4}	10^{-4}	10^{-3}
Online computer	PDP11/34	PDP11/24	PC8000

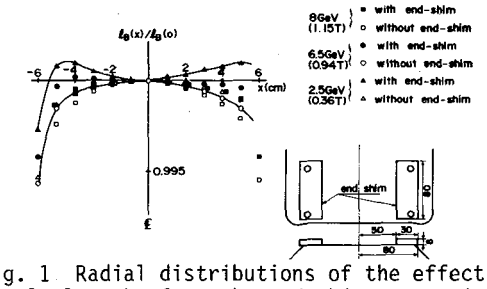

Fig. 1 Radial distributions of the effective dipole length after the end shim correction.

Dipole The radial distributions of the effective dipole length are shown in Fig. 1. The slight correction of the field was made attaching the simple shims shown in the same figure at both magnet ends. The effective length increased by 0.01 ∿ 0.02 % at the both aperture ends and the almost flat distribution was obtained.
The statistical distribution of the effective lengths at 6.5 GeV is given in Fig. 2(a). The standard deviation is 0.038 % reflecting mainly the core length distribution rather than the gap height errors and the permeability fluctuations. The effective length distribution of the remanent field (Fig. 2(d)) reflects the variation of the coercive force.

Quadrupole The radial distribution of the effective length of the field gradient had to be corrected due to the large variation in the aperture as shown in Fig. 3. The best correction was found after trying various types of the laminated shims at all pole ends. Several results are shown in Fig. 3 with the shim structure. Applying the shims thus determined, it was possible to level the radial distribution within ± 0.01 % in the aperture.

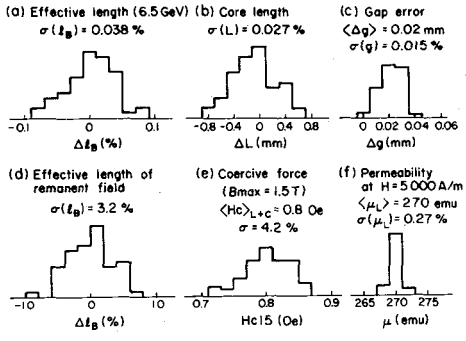

Fig. 2 Statistical distributions of the effective dipole length, fabrication errors and magnetic properties of the silicon steel H23 (S23 grade) for the dipoles.

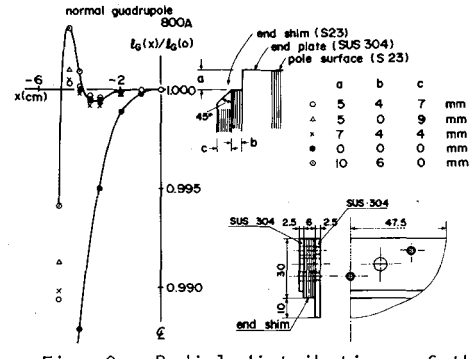

Fig. 3 Radial distributions of the effective quadrupole length after the various end shim corrections for the normal quadrupoles.

The effective lengths of the field gradients of the normal quadrupoles distribute statistically as shown in Fig. 4(a). Their standard deviation is 0.089 % reflecting also the core length distribution. This value corresponds to the thickness of a sheet of the lamination. The mechanical deviations of the bore diameters are within the tolerable limit and the symmetry of 4 poles is satisfactory. The mechanical differences of the minimum gap heights at the horizontal and vertical planes are 0.003 ± 0.015 mm and 0.002 ± 0.015 mm, respectively. The field gradient error arising from the pole asymmetry is ignorable. The effective lengths of the remanent

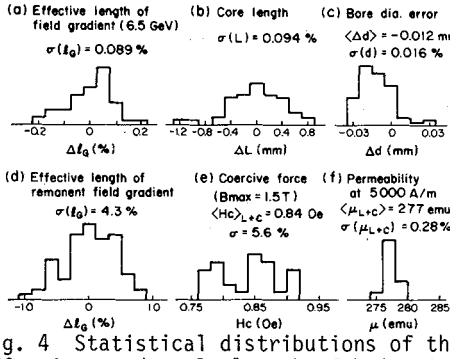

Fig. 4 Statistical distributions of the effective quadrupole length, fabrication errors and magnetic properties of the silicon steel RM23 (S23 grade) for the normal quadrupoles.

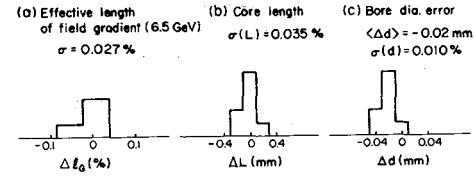

Fig. 5 Statistical distributions of the effective quadrupole length and fabrication errors for the insertion quadrupoles.

field gradients are given in Fig. 4(d). Their variation also reflects the distribution of the coercive force.
For the insertion quadrupoles, the similar statistical distributions are given in Fig. 5. The steel properties are same as Fig. 4. The asymmetries of the poles measured at the minimum gaps are 0.015 ± 0.013 mm horizontally and 0.003 ± 0.010 mm vertically. The effective length of one quadrupole was smaller by 0.2 % and was corrected by increasing the thickness of the pole end shims. Fig. 5(a) was obtained after this correction.

Sextupole The effective lengths of the sextupole field of Table 3 were obtained

Table 3 Effective length of the sextupole

	core length (mm)	effective sextupole length (mm)		
		30A	80A	100A
SXF	170	191	190	191
SXD	270	274	278	278

Table 4 Effective lengths of steering dipoles

	STV 1	STV 2	STH 1	STH 2
gap height (mm)	130	154	70	154
eff. length (mm)	356	214	275	291

from the field mapping of each type of the sextupoles. The two dimensional distributions of all sextupoles were measured at the longitudinal centers of the magnets. Fig. 6 shows the results with the fabrication errors. The variation of the core lengths is very small and the distribution of the effective sextupole lengths may be estimated from Fig. 6(a).

Steering dipole The iron core was not laminated but the ramped excitation from 0 to 10 A during 10 sec did not show the field deterioration due to the eddy current. The effective lengths of each type are given in Table 4.

III - SPECULATIONS ON BEAM PROPERTIES

Estimating from the effective length variation, the closed orbit distortion is about 1 mm at 6.5 GeV. Other sources of the distortion are the alignment errors of the quadrupoles, stray field and the tilts of the dipoles. Taking these sources into consideration, a few mm of the orbit distortion will be expected.
For the storage accelerator, it usually takes for a long time to accumulate the intense beam. Sometimes the mis-tuning of the accelerator happens to lose the stored beam. It is desirable to keep the beam loss at a minimum. To attain the highly reliable machine, the beam should remain at the same condition if it displaced within the aperture. The effective length distributions of Fig. 1 and Fig. 3 after the corrections with the pole end shims will assure this condition.

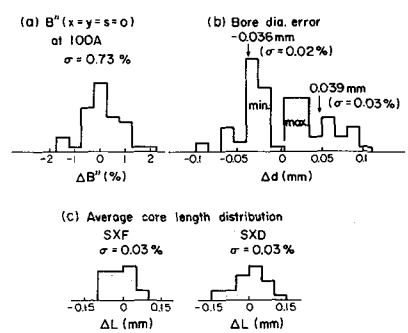

Fig. 6 Statistical distributions of the sextupole strength and fabrication errors.

The width of the half integral stopband estimated from the effective gradient length of Fig. 4(a) is 0.02. It is fairly small. The tune shifts are estimated to be less than 0.0002 for both the horizontal and vertical motions from the octupolar field deterioration estimated from Fig. 3 after the shim correction. The horizontal and vertical tune spreads due to the chromatic aberration are ± 0.02 and ± 0.03 at 6.5 GeV, respectively. Both spreads can be compensated with the sextupoles which are excited in 4 families.

References

1) K. Endo, H. Fukuma, A. Kabe, Ta. Kubo, To. Kubo, N. Kumagai and Y. Takeuchi, KEK Internal 82-10 (1982).
2) N. Kumagai, Y. Takeuchi and K. Endo, IEEE Trans. MAG-17 (1981) 1606.